Non-invasive diffuse optical monitoring of cerebral physiology in an adult swine-model of impact traumatic brain injury

RODRIGO M. FORTI,[1,2,*] (ID) LUCAS J. HOBSON,[2,3] EMILIE J. BENSON,[1,4] TIFFANY S. KO,[2,3] NICOLINA R. RANIERI,[1,2] GERARD LAURENT,[1,2] M. KATIE WEEKS,[2,3] NICHOLAS J. WIDMANN,[2,3] SARAH MORTON,[2,3] ANTHONY M. DAVIS,[2,3] TAKAYUKI SUEISHI,[2,3] YUXI LIN,[2,3] KARLI S. WULWICK,[2,3] NICHOLAS FAGAN,[2,3] SAMUEL S. SHIN,[2,5] SHIH-HAN KAO,[2,3] DANIEL J. LICHT,[1,5] BRIAN R. WHITE,[5,6] (ID) TODD J. KILBAUGH,[2,3,5] ARJUN G. YODH,[4] AND WESLEY B. BAKER[1,2,5]

[1]*Division of Neurology, Children's Hospital of Philadelphia, Philadelphia, PA 19104, USA*
[2]*Resuscitation Science Center of Emphasis, CHOP Research Institute, Philadelphia, PA 19104, USA*
[3]*Department of Anesthesiology and Critical Care Medicine, Children's Hospital of Philadelphia, Philadelphia, PA 19104, USA*
[4]*Department of Physics and Astronomy, University of Pennsylvania, Philadelphia, PA 19104, USA*
[5]*Perelman School of Medicine, University of Pennsylvania, Philadelphia, PA 19104, USA*
[6]*Division of Cardiology, Children's Hospital of Philadelphia, Philadelphia, PA 19104, USA*
[*]*menezesfor@chop.edu*

Abstract: In this study, we used diffuse optics to address the need for non-invasive, continuous monitoring of cerebral physiology following traumatic brain injury (TBI). We combined frequency-domain and broadband diffuse optical spectroscopy with diffuse correlation spectroscopy to monitor cerebral oxygen metabolism, cerebral blood volume, and cerebral water content in an established adult swine-model of impact TBI. Cerebral physiology was monitored before and after TBI (up to 14 days post injury). Overall, our results suggest that non-invasive optical monitoring can assess cerebral physiologic impairments post-TBI, including an initial reduction in oxygen metabolism, development of cerebral hemorrhage/hematoma, and brain swelling.

1. Introduction

Traumatic brain injury (TBI) is a leading cause of morbidity and mortality in the United States [1–3]. After the primary insult, a cascade of secondary cerebral physiologic derangements (*e.g.,* hypoperfusion, hyperemia, seizure, edema) can lead to secondary brain damage that worsens outcomes [4,5]. Important clinical care decisions for the mitigation of secondary injury include: (1) management of arterial blood pressure, systemic CO_2, and sedation to prevent ischemic and hyperemic conditions; (2) assessment of the need for and efficacy of therapies to treat cerebral edema and elevated intracranial pressure (ICP) [5,6]. To manage TBI patients, clinicians typically rely on systemic measurements (*e.g.,* mean arterial pressure, P_aCO_2, arterial oxygen saturation, serum pH) coupled with serial neurologic examinations [5,6]. Systemic physiology, however, may not provide a complete picture of the cerebral physiologic status of individual patients. In current clinical care, methodologies to provide continuous, bedside, noninvasive information about cerebral health are lacking. Imaging, as with computed tomography (CT), can assess for cerebral edema, hemorrhage, and brain herniation, but such imaging can only be performed intermittently, and therefore irreversible secondary injury can go undetected. Invasive regional

brain monitors (*e.g.,* intracranial pressure, brain tissue oxygen tension) [5,7–9] are the standard of care in some institutions for severe patients, but the complexities and associated risks with their placement limit their use. This is especially true in pediatrics where multi-modal intracranial monitoring is infrequent even in severe TBI.

Diffuse optics technology holds promise for non-invasive detection of cerebral hypoperfusion, hyperemia, edema, hemorrhage, and metabolic dysfunctions at the bedside [10–14], which holds potential to aid clinical decision-making. Continuous-wave (CW) diffuse optical spectroscopy (also known as near-infrared spectroscopy, NIRS) has been previously used to monitor regional cerebral tissue oxygenation in patients after TBI, but concerns about the accuracy of CW-NIRS exist [13,14]. More advanced diffuse optical instruments have been proposed for accurately monitoring physiology in numerous clinical populations [10,11,15]. In prior studies, the combination of broadband diffuse optical spectroscopy (bDOS) and frequency-domain diffuse optical spectroscopy (FD-DOS) has been used to measure oxygenation, hemoglobin concentration, and water and lipid content in breast, adipose, and muscle tissues [16–22]. A few studies have also demonstrated the integration of diffuse correlation spectroscopy (DCS) with bDOS [16–19], as well as the integration of DCS with FD-DOS [20–27] for cerebral monitoring of blood flow and oxygen metabolism. Another prior study integrated FD-DOS, DCS, and bDOS to monitor breast tumor blood flow, oxygenation, and oxygen metabolism during neoadjuvant chemotherapy [28].

In this study, we report the first application of integrated FD-DOS/DCS/bDOS technology for neuromonitoring in a high-fidelity adult swine model of impact TBI. Specifically, we performed proof-of-concept longitudinal measurements of cerebral blood flow (CBF), cerebral metabolic rate of oxygen (CMRO$_2$), oxygen extraction fraction (OEF), tissue hemoglobin concentration (HbT), tissue water volume fraction (f_{H_2O}), and tissue lipid fraction (f_{Lipid}) in adult swine in the two weeks following impact TBI. Notably, since the initial injury is typically followed by brain swelling (i.e., an increase in tissue water content over time), and intracranial hypertension [4,29], we hypothesized that the optical measurements would show increased f_{H_2O} following injury. Further, since TBI can lead to an acute hypoperfusion/ischemia phase, potentially associated with a metabolic failure and cerebral hemorrhage [4,30,31], we also hypothesized that the optical measurements would exhibit diminished CBF and CMRO$_2$ with elevated OEF and HbT in the acute phase after injury.

2. Methods

2.1. Experimental design

In this study, we performed observational measurements on pigs that were subjects in preclinical trials to understand the injury mechanisms of TBI, including a preclinical prospective cohort study of an experimental mitochondrial-targeted therapeutic drug for TBI. Observational measurements were performed based on availability of personnel and were not associated with experimental parameters, and treatment was not considered as a variable of interest in the present study. In total, we monitored fourteen subjects before and after impact TBI with FD-DOS/DCS/bDOS. Animals were anesthetized via intramuscular injection of ketamine (20 mg/kg) and xylazine (2 mg/kg). Animals were then intubated, and anesthesia was maintained with inhaled isoflurane (∼2%). Anesthesia was adjusted as needed to ensure the absence of withdrawal to a firm hoof pinch. Following intubation, we administered a dose of Cefazolin (25 mg/kg) for surgical prophylaxis and shaved the head of the animals.

Once stable, the right coronal suture was exposed, and a circular craniectomy approximately 3 cm in diameter was made over the rostral gyrus. Then, we removed the dura matter to expose the cortical surface and we secured the injury device to the head. The injury was induced using a controlled cortical impact (CCI) device, *i.e.,* a skull-mounted, spring-loaded blunt indentation device (Fig. 1(a), for a more in-depth description of the CCI device, please refer to
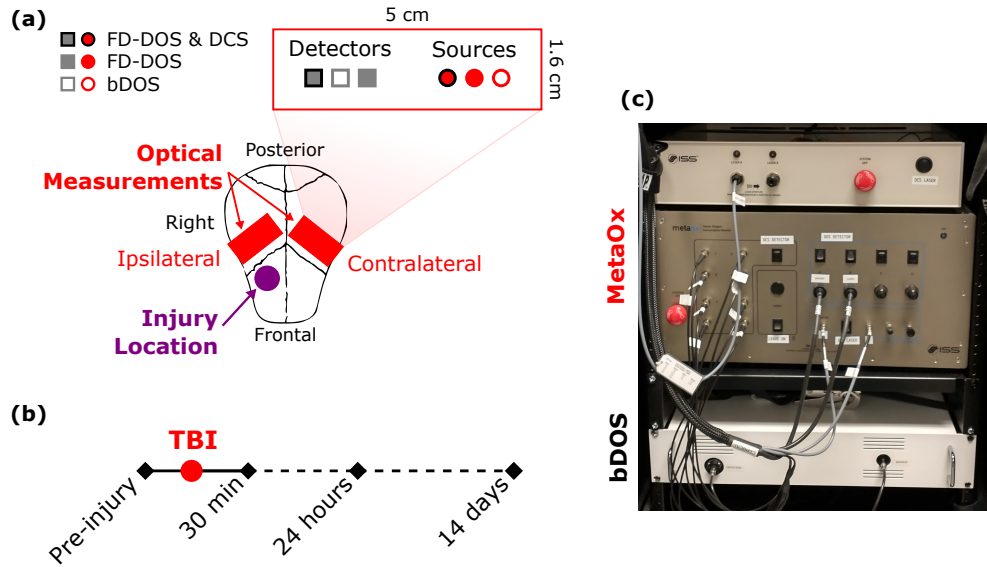
Fig. 1. **(a)** Schematic of the optical probe and the locations of the bilateral optical measurements. The optical probe comprised 4 source-detector separations (SDS) for frequency-domain diffuse optical specotrscopy (FD-DOS, 1.5, 2.0, 2.5, 3.0 cm), a single SDS for diffuse correlation spectorscopy (DCS, 2.5 cm), and a single SDS for broadband DOS (bDOS, 3.0 cm). Mild-to-moderate focal contusion traumatic brain injury (TBI) was induced using a controlled cortical impact device in adult-aged swine (the skull and dura were permanently removed at the injury location). **(b)** Timeline of the study's pre- and post-injury bilateral optical measurements. **(c)** Image of the instrument showing the commercial MetaOx (which combines FD-DOS and DCS), and our lab built bDOS instrument.

[32]). This model provides a well-defined and reproducible cortical and subcortical contusion that is reminiscent of human TBI and can be modulated to vary in severity [32–35]. We induced a mild-to-moderate injury by rapidly (~400 ms, 7-9 mm depth) firing the spring loaded indentor tip to deform approximately 1 cm^3 of cortical tissue. Immediately after the injury, the skin flaps were sutured closed, the dura was re-approximated, but the removed portion of the skull was not re-inserted [32]. Animals were extubated and returned to the animal housing facility.

Using our FD-DOS/DCS/bDOS device, we sequentially measured each brain hemisphere (Fig. 1(b)) immediately before injury, and at 30 minutes, 24 hours, and 14 days post injury (Fig. 1(c)). To avoid the location of the cranial incision, we carried out the hand-held optical spot measurements posterior to the injury on the ipsilateral hemisphere, and at a symmetric location on the contralateral hemisphere. As an attempt to standardize the measurement locations, we positioned the optical probes using anatomical features of the pig skull (i.e., immediately lateral to the midline and posterior to the coronal suture). Animals were sedated prior to all optical measurements (using the same anesthesia procedure described above). Structural magnetic resonance imaging (MRI) was obtained at 24 hours and 14 days post-injury. All procedures were approved by the Institutional Animal Care and Use Committee of the University of Pennsylvania and performed in accordance with the National Institutes of Health Guide for the Care and Use of Laboratory Animals.

2.2. Diffuse optical measurements

The FD-DOS/DCS/bDOS device consists of a customized version of a commercially-available FD-DOS/DCS system (MetaOx, ISS Medical, USA) [36] and a custom-built bDOS module (Fig. 1(c)). Our FD-DOS/DCS device uses two multi-wavelength intensity-modulated FD-DOS sources (110 MHz modulation frequency, 680, 760, 805, 830 nm wavelengths), two FD-DOS detectors, two DCS sources (850 nm wavelength), and 8 DCS detectors. To permit simultaneous FD-DOS and DCS data collection, the MetaOx uses a short-pass spectral filter in front of the FD-DOS detectors to block DCS source light. The combined sampling frequency for FD-DOS/DCS was 50 Hz. Of note, the DCS detector bundles were sufficiently far from the FD-DOS sources that there was minimal FD-DOS source light contamination in the DCS measurements (*i.e.,* no filter was needed in front of the DCS detectors to block the FD-DOS light).

The bDOS module uses a fiber-coupled halogen lamp (HL-2000-HP-FHSA, Ocean Optics, USA) and a fiber-coupled f/1.5 spectrometer (TEC Cooled to $-15°$ C, integrated 100 micron slit; Wasatch Photonics, USA) to measure the tissue diffuse reflectance in the 650-1000 nm spectral range (4.8 nm spectral resolution). The spectrometer integration time was set to 100 ms. During bDOS monitoring, the tissue diffuse reflectance and dark counts were sequentially obtained every 2s: each tissue diffuse reflectance and dark count measurement was time-averaged for 1 second (an optical shutter in front of the halogen lamp was used to obtain the dark counts).

The FD-DOS/DCS/bDOS probe comprised 4 source-detector separations (SDS) for FD-DOS (1.5, 2.0, 2.5, 3.0 cm), a single SDS for DCS (2.5 cm), and a single SDS for bDOS (3.0 cm). The surface of the optical probe ìn contact with the head was approximately 5 cm x 1.6 cm (Fig. 1(a)). To avoid cross-contamination between FD-DOS/DCS and bDOS, the measurements were manually interleaved. Specifically, each cerebral hemisphere was sequentially monitored with FD-DOS/DCS for 3 minutes and bDOS for 1 minute; the probe was manually held against the skin. Then, the probe was placed on a silicon phantom with known optical properties to determine the FD-DOS light coupling coefficients [11,37]. After the FD-DOS calibration, the probe was secured to a spectrally flat reflectance standard (SRS-40-020, Labsphere, USA) via a custom 3D-printed probe holder to measure the spectral response function of our bDOS light source and detector.

2.3. Diffuse optical analysis algorithm

A flow chart of the analysis algorithm used to recover CBF, CMRO$_2$, OEF, HbT, f_{H_2O}, and f_{Lipid} is shown in Fig. 2. All the analysis was performed using MATLAB R2022a (Mathworks, USA). The FD-DOS/bDOS component of the algorithm closely resembles an algorithm previously used for human breast tissue measurements [38].

First (step 1 in Fig. 2), we recovered the absorption ($\mu_{a,\,FD}(\lambda_{FD})$) and reduced scattering ($\mu'_{s,FD}(\lambda_{FD})$) coefficients at the FD-DOS wavelengths (λ_{FD} =680, 760, 805, 830 nm). As described elsewhere [11,37], each multi-distance FD-DOS amplitude and phase measurement was fit to the long SDS approximation of the semi-infinite photon diffusion equation solution for the tissue optical properties. Optical properties derived from linear fits with $R^2 < 0.9$ were excluded. To avoid motion artifacts, $\mu_{a,FD}$ and $\mu'_{s,FD}$ were calculated from the temporal averages of the amplitude and phase measurements during the last 20 seconds of FD-DOS data acquisition. The resulting multispectral $\mu'_{s,FD}$ values were next fit to a power function of the form:

$$\mu'_s(\lambda) = A(\lambda/500\ nm)^{-b}. \tag{1}$$

To recover the scattering amplitude, *A*, and the scattering power, *b*, from Eq. (1), we used a constrained nonlinear minimization algorithm implemented in MATLAB (*fminsearchbnd*); *A* and *b* were constrained to be between 0 and 100 cm^{-1} and between 0.45 and 2, respectively.

To calibrate the bDOS data (step 2 in Fig. 2), we corrected each tissue diffuse reflectance spectrum measurement ($R_{raw}(\lambda, t)$) by subtracting its associated dark count ($R_{dark}(\lambda, t)$). We then
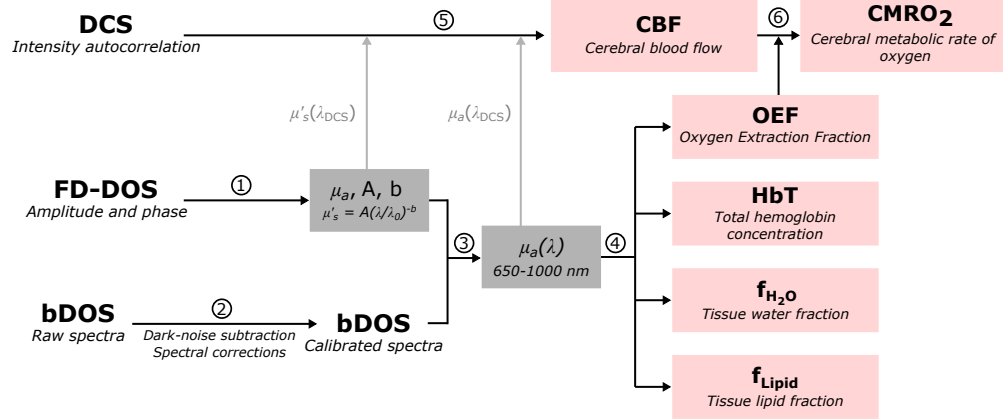
Fig. 2. Flow chart of the analysis algorithm for the integrated diffuse correlation spectroscopy (DCS), frequency-domain diffuse optical spectroscopy (FD-DOS), and broadband diffuse optical spectroscopy (bDOS) data. The tissue absorption and reduced scattering coefficients at wavelength λ are $\mu_a(\lambda)$ and $\mu'_s(\lambda)$, A is the scattering amplitude, and b is the scattering power (from Eq. (1), i.e., $\mu'_s(\lambda) = A(\lambda/\lambda_0)^{-b}$, with $\lambda_0 = 500$ *nm*).

time-averaged these dark-corrected spectra across the 1-minute bDOS data acquisition period, *i.e.,* $R_1(\lambda) \equiv \langle R_{raw}(\lambda, t) - R_{dark}(\lambda, t) \rangle$. Next, $R_1(\lambda)$ was divided by the reflectance standard measurement ($R_{RefStd}(\lambda)$) to account for the spectral response of the bDOS instrument (*i.e.,* $R_2(\lambda) \equiv R_1(\lambda)/R_{RefStd}(\lambda)$). The true tissue diffuse reflectance emerging from tissue ($R(\lambda)$) is the product of $R_2(\lambda)$ and the bDOS system's light coupling coefficient (R_0).

The last step in the bDOS calibration is to measure R_0 from the FD-DOS measurement of the optical properties; for this we assumed that R_0 does not depend on wavelength. Specifically, using an assumed wavelength-independent tissue index of refraction and effective Fresnel reflection coefficient of $n = 1.4$ and $R_{eff} = 0.0065$ (we assumed an index of refraction of black plastic for the outside medium, i.e., $n_{out} = 1.45$), respectively, and using the $\mu_{a,FD}(\lambda_{FD})$ and $\mu'_{s,FD}(\lambda_{FD})$ measurements, we evaluated the semi-infinite continuous-wave photon diffusion equation solution [11] to obtain the theoretical reflectance at the FD-DOS wavelengths, *i.e.,* $R_{theory}(\lambda_{FD})$. R_0 was then computed by solving the following linear system of equations (using the *lscov* function from MATLAB):

$$\begin{pmatrix} R_2(\lambda_{FD,1}) \\ \vdots \\ R_2(\lambda_{FD,4}) \end{pmatrix} \times R_0 = \begin{pmatrix} R_{theory}(\lambda_{FD,1}) \\ \vdots \\ R_{theory}(\lambda_{FD,4}) \end{pmatrix}. \tag{2}$$

Finally, the calibrated bDOS spectrum was calculated as $R(\lambda) = R_0 \times R_2(\lambda)$.

The third step in the analysis algorithm is the derivation of the tissue absorption coefficient spectrum ($\mu_a(\lambda)$) across the entire 650-1000 nm range (step 3 in Fig. 2). First, using the recovered A and b from step 1, we estimated $\mu'_s(\lambda)$ across the 650-1000 nm range using Eq. (1). Then, for each λ, $R(\lambda)$ was fit to the semi-infinite continuous-wave photon diffusion equation solution to extract $\mu_a(\lambda)$ ($\mu'_s(\lambda)$, $n = 1.4$ and $R_{eff} = 0.0065$ were inputs for this fit). The fit was performed using the *fminserachbnd* fuction, with $\mu_a(\lambda)$ constrained between 0.001 and 1 cm^{-1}.

Step 4 in Fig. 2 is estimating the tissue concentrations of oxy- and deoxy-hemoglobin (HbO and HbR, respectively), and tissue fractions of water (f_{H_2O}) and lipid (f_{Lipid}), from their known spectral extinction coefficients and the bDOS $\mu_a(\lambda)$ spectrum [10,11]. The total tissue

hemoglobin concentration was $HbT = HbO + HbR$ and the oxygen extraction fraction was $OEF = 100/\gamma \times (1 - StO_2)$, where γ is the venous/arterial ratio of blood monitored by bDOS (assumed to be 0.75) [39], and $StO_2 = HbO/HbT$ is the tissue oxygen saturation. Our OEF derivation assumed that the arterial oxygen saturation was 100%, which is reasonable given that animals were mechanically ventilated.

Step 5 in Fig. 2 is extracting a CBF index from the nonlinear fit of the mean DCS intensity autocorrelation function measurement (i.e., $\langle g_2(\tau) \rangle$, $\langle \rangle$ denotes the mean across the last 20 seconds of DCS data acquisition for each delay-time) to the semi-infinite correlation diffusion equation solution [11,12]. To increase the measurement sensitivity to blood flow at deeper tissue depths, we restricted our fits to the portion of the autocorrelation curves where $g_2(\tau) \geq 1.15$ [40,41]. Inputs for the fit included the $\mu_a(\lambda_{DCS})$ and $\mu_s'(\lambda_{DCS})$ measurements from steps 1 and 3 at the DCS wavelength ($\lambda_{DCS} = 850\ nm$).

The final step of the algorithm (step 6 in Fig. 2) was computing the product of CBF and OEF to obtain a cerebral metabolic rate of oxygen index (CMRO$_2$). This index can be used to measure fractional changes in CMRO$_2$ if the arterial blood concentration of oxygen and the venous/arterial ratio of blood monitored by bDOS remain constant over time [20,39].

2.4. Statistical analysis

Summary statistics are presented using medians and interquartile ranges. All statistical tests were 2-sided, and $p < 0.05$ indicates significance. For each hemisphere, we examined pre-TBI to post-TBI changes in optically measured CBF, CMRO$_2$, OEF, HbT, f_{H_2O}, A, and b. For each of these variables, the Wilcoxon Signed-rank test was used to assess for differences between pre-injury values and their values at each post-TBI timepoint (*i.e.*, 30 minutes, 24 hours, 14 days).

3. Results

Of the 14 subjects in the cohort, diffuse optical measurements were not performed at 24 hours and 14 days post-injury in two subjects; of these two subjects, one experienced complications prior to the 24 hours timepoint that required euthanasia, and for the other subjects the FD-DOS/DCS/bDOS instrument was not available. In addition, 3 of the 14 subjects were administered the study drug at 1-hour post-injury. To avoid confounders from the drug, the measurements at 24 hours and 14 days post-injury were excluded in these subjects. Accordingly, we analyzed the data acquired in all 14 subjects for the pre-injury and 30 minutes post-injury timepoints, and the data acquired in 9 subjects for the 24 hours and 14 days post-injury timepoints. After data processing, we encountered data quality issues that prevented the recovery of the ipsilateral cerebral metrics at the 30 minutes post-injury timepoint in one subject and at the 14 days post-injury timepoint in another subject; these two ipsilateral measurements were thus excluded from all subsequent analyses. The pre-injury cerebral physiologic measurements are summarized in Table 1. Example results for the $\mu_a(\lambda)$ and $\mu_s'(\lambda)$ fits are shown in Fig. S1.

Initially, we hypothesized that we would encounter diminished CBF and CMRO$_2$ with elevated OEF and HbT in the acute phase after injury We observed significant ipsilateral reductions in CBF ($p = 0.006$) and CMRO$_2$ ($p = 0.001$) and a significant ipsilateral elevation in HbT ($p = 0.048$) at 30 minutes post-injury (Fig. 3). Contrary to our hypothesis, however, significant alteration in ipsilateral OEF was not observed (Fig. 3). In the contralateral hemisphere, there was no significant pre-injury to post-injury alterations in any of these variables. At 24 hours post-injury, ipsilateral HbT remained significantly elevated ($p = 0.008$). CBF and CMRO$_2$ exhibited a trending decrease relative to their pre-injury levels, but these reductions were not significant. At 14 days post-injury, ipsilateral CBF, CMRO$_2$, and HbT recovered to pre-injury levels. Importantly, the results for StO$_2$ are analogous to the OEF results since they are directly related.

In contrast to our f_{H_2O} hypothesis (i.e., increased f_{H_2O} after TBI due to brain swelling), we observed a transient *reduction* in f_{H_2O} at 30 minutes post-injury (Fig. 4), for both the ipsilateral

Table 1. Pre-injury diffuse optical metrics of cerebral physiology. Median [IQR] ($n = 14$)

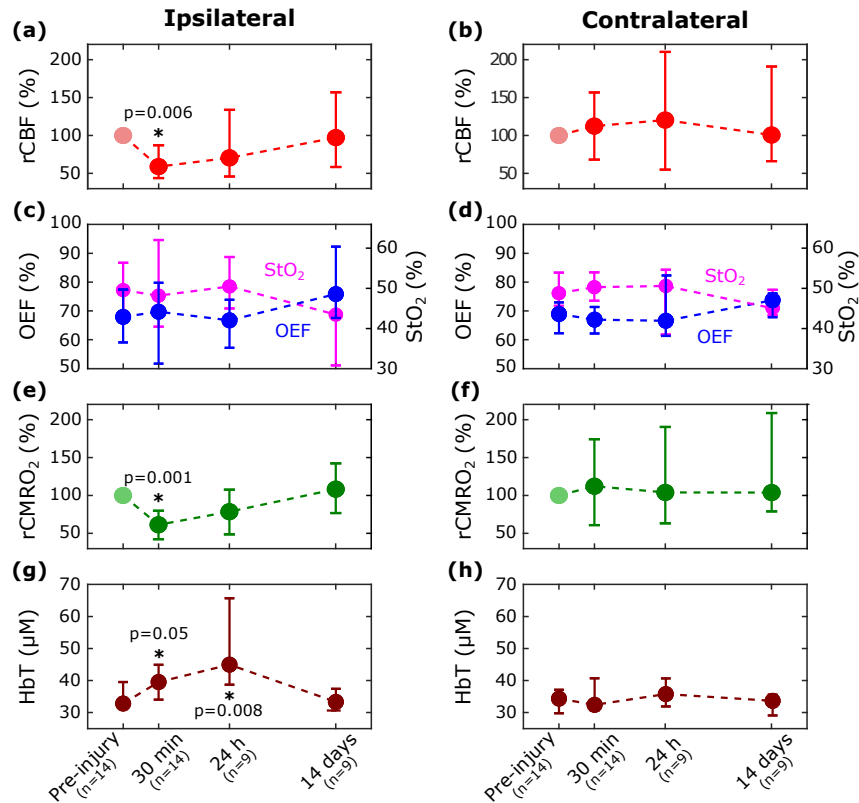|	Ipsilateral	Contralateral
CBF ($\times 10^{-8} cm^2/s$)	0.93 [0.60, 1.66]	0.89 [0.57, 1.24]
HbT (μM)	33 [31, 40]	34 [30, 37]
StO$_2$ (%)	49 [42, 56]	48 [45, 53]
OEF (%)	68 [59, 77]	68 [62, 73]
CMRO$_2$(a.u.)	59 [43, 101]	49 [36, 74]
f$_{H_2O}$ (%)	59 [55, 64]	66 [63, 69]
f$_{Lipid}$(%)	9.6 [6.8, 11.5]	9.0 [4.5, 16.6]
A (cm^{-1})	12.0 [10.6, 12.8]	11.0 [10.2, 13.4]
b	0.94 [0.87, 1.18]	0.94 [0.85, 1.04]

Fig. 3. Pre- and post-injury diffuse optical measurements of relative cerebral blood ($rCBF \equiv 100 \times CBF/CBF_0$), oxygen extraction fraction (OEF), oxygen saturation (StO$_2$), relative cerebral metabolic rate of oxygen ($rCMRO2 \equiv 100 \times CMRO_2/CMRO_{2,0}$), and tissue hemoglobin concentration (HbT) for the ipsilateral (first column) and contralateral (second column) hemispheres. rCBF and rCMRO$_2$ are normalized to their pre-injury levels, *i.e., CBF$_0$* and *CMRO$_{2,0}$*. The medians (circles) and interquartile ranges (error bars) across subjects for each measurement timepoint are shown. *P* values indicate whether the median pre-injury to post-injury change was different from zero.

Fig. 4. Pre-injury and post-injury diffuse optical measurements of cerebral tissue water volume fraction (f_{H_2O}), scattering amplitude (A), and scattering power (b) for the ipsilateral and contralateral hemispheres (A and b are defined by Eq. (1)). The medians (circles) and interquartile ranges across subjects for each measurement timepoint are shown. P values indicate whether the median pre-injury to post-injury change was different from zero.
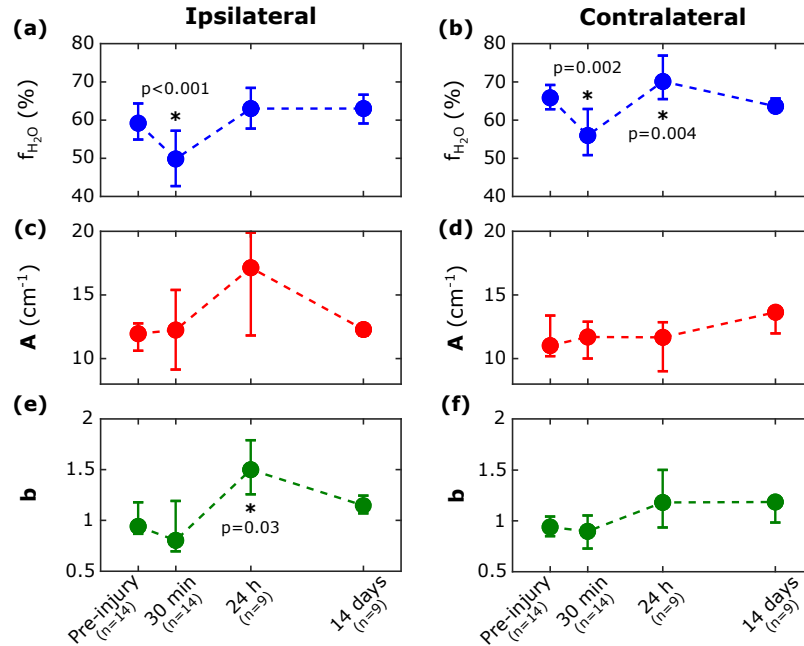
($p < 0.001$) and contralateral ($p = 0.002$) hemispheres. Ipsilateral f_{H_2O} appeared to return to the pre-injury level at 24 hours ($p = 0.2$) and remained there at 14 days post-injury. Contralateral f_{H_2O} exceeded its pre-injury level at 24 hours ($p = 0.004$) and returned to pre-injury levels at 14 days post-injury.

Finally, there were pre-injury to post-injury changes in tissue scattering at 24 hours post-injury (Fig. 4). Specifically, the ipsilateral scattering parameter b was significantly increased ($p = 0.03$), and there were trending but not significant increases in the ipsilateral A ($p = 0.10$) and contralateral b ($p = 0.13$) scattering parameters. There were no pre-injury to post-injury changes in tissue scattering at 30 minutes post-injury and 14 days post-injury. The MRI scans at both 24 hours and 14-days post-injury revealed significant brain contusion and injury in all subjects (see an example in Fig. 5), likely due to the cranial incision used to induce TBI.
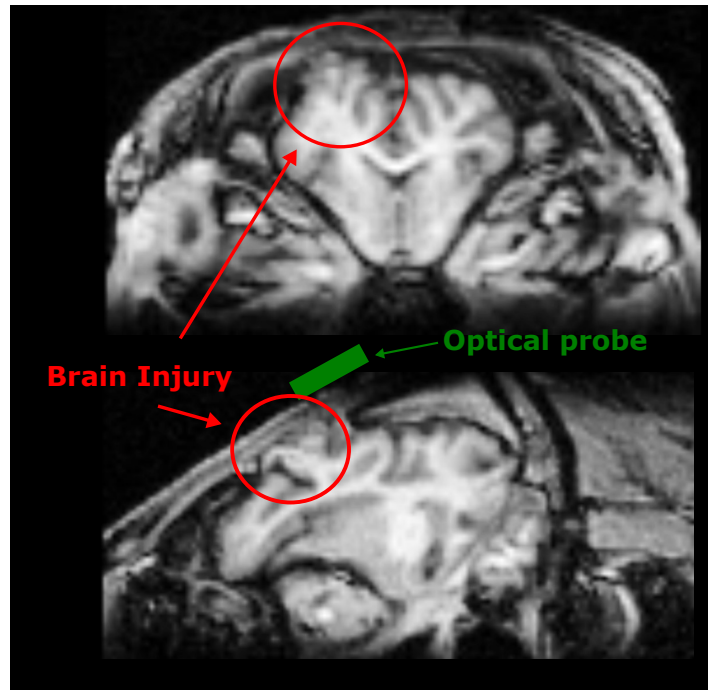
Fig. 5. – An exemplar structural MRI image collected at 24 hours post injury, revealing significant brain contusion and injury at the injury location (red circle). Here, we also represent the approximate location of the optical measurements (in green); to avoid the cranial incision we always placed our optical probes in a region posterior to the injury site.

4. Discussion

Diagnosing and monitoring the evolution of the secondary injury pathways are one of the most challenging aspects of the clinical management of TBI as the secondary insults and their associated injury mechanisms evolve differently for each patient. Placement of intracranial monitors has inherent risks, requires specialized providers for placement, and is not performed in the field or in austere settings. Non-invasive multi-modal neuromonitoring solves many of these issues. For example, intracranial pressure may be caused by different factors, including cerebral hemorrhage/hematoma, cerebral edema, and hyperemia [4,6,29], each requiring different treatment strategies. By measuring multiple cerebral physiological parameters, diffuse optical methods hold promise for aiding in the timely diagnosis of secondary damage pathways in real-time at the bedside, allowing for development of individualized treatment strategies. In this study, we presented preliminary evidence about the utility of using an integrated FD-DOS/DCS/bDOS system to assess cerebral pathophysiology after TBI in swine. Our results showed evidence of cerebral hemorrhage/hematoma and metabolic failure acutely after TBI on the ipsilateral hemisphere. In addition, our results may also suggest that optics is capable of non-invasively assessing brain swelling at 24 hours post-injury.

4.1. Cerebral pathophysiology at 30 minutes post-injury

Prior invasive and non-invasive neuromonitoring data obtained in pediatric swine models of closed-head diffuse TBI found reduced CBF, reduced cerebral oxygenation (or elevated OEF), and elevated HbT at 30 minutes post-injury [30,31]. In our study, we also observed a decrease in ipsilateral CBF and $CMRO_2$, but we did not see an increase in OEF (or a decrease in StO_2).

Although we observed a large variability in OEF, the matching decrease in $CMRO_2$ and CBF without changes in OEF may suggest a metabolic failure following TBI, which was accompanied by a matching drop in oxygen delivery. This metabolic failure is likely explained by a failure of oxidative respiration due to mitochondrial injury and thus reduced uptake of oxygen. Importantly, the degree of metabolic failure after TBI is thought to be related to the severity of the primary injury, and may be related to functional outcomes [4,42].

Surprisingly, instead of observing the hypothesized acute increase in f_{H_2O} (indicative of the expected edema formation [43,44]), we observed a global decrease in f_{H_2O} immediately following TBI. Although we are uncertain of the exact reason for this initial decrease in cerebral water content, our observation might be explained by transient cerebral spinal fluid (CSF) leakage through the cranial incision used to induce injury. Since CSF is capable of crossing between the brain's hemispheres, a CSF leak may explain why this decrease was seen in both the ipsilateral and contralateral hemispheres.

Consistent with prior work, we observed an ipsilateral elevation in HbT at 30 minutes post-injury [30]. This may reflect increased tissue blood volume fraction in the ipsilateral hemisphere. Generally, an increase in tissue blood volume could arise from hemorrhage/hematoma, increased cerebral blood flow, or inflammation. The presence of blood outside the vascular compartment is often the case in hemorrhage and hematoma; hemorrhages are active brain bleeds from burst blood vessels, and hematomas describe a mass of usually clotted blood. Inflammation is a natural immune response to injuries and infections that may also be accompanied by a transient increased blood volume and blood flow [4,45]. Since we observed a decrease in CBF at 30 minutes post injury, the observed increase in HbT may be indicative of hemorrhage and/or hematoma on the ipsilateral hemisphere.

Although it is puzzling that we observed no changes in OEF (or StO_2), prior work has observed that hemorrhages/hematomas can contain substantial amounts of oxygenated hemoglobin during the hyperacute phase (<12 h) [46]. Finally, the presence of hematomas can confound the OEF calculations in a way that masks cerebral ischemia (e.g., the influence of an increased OEF in vascularized ischemic tissue on the optical signals may be counteracted by the influence of a hematoma with mostly oxygenated blood). Future studies are needed to further examine the influence of cerebral hemorrhages/hematomas on the HbT/StO_2 changes.

The use of CW-NIRS to measure cerebral hematomas has been previously explored in multiple studies, and there is currently an FDA-approved device for this application based on CW-NIRS (InfraScan Inc, Philadelphia, PA, USA) [47,48]. This device detects cerebral hematoma by measuring the hemispheric difference in optical density at a few near-infrared wavelengths; this difference is expected to be associated with differences in HbT. However, this approach does not allow for the absolute quantification of HbT and does not provide information about CBF. Our finding of increased HbT at 30 minutes post-TBI further support the use of diffuse optics to non-invasively diagnose the presence of cerebral hemorrhage/hematoma. Moreover, by additionally measuring CBF, our methodology may further improve the sensitivity and specificity of the optical detection of hematoma by allowing the differentiation of the causes of elevated HbT. However, it is desirable for future studies to validate our approach with larger sample sizes and with direct gold-standard measurements of the presence/extent of the hematomas.

It is important to note that animals used in this study had a mild-to-moderate injury. Although some animals may have had some neurologic sequelae, all subjects were able to return to the animal facility without need for intensive care. In current clinical practice, most patients that present to the hospital with mild to moderate injuries, without clear evidence of neurological deficits are discharged without additional neuromonitoring/neuroimaging [49,50]. Although instruments based on these optical measurements are unlikely to replace CT imaging, the current gold-standard for detection of hemorrhages, hematomas, and edema, a combination of CT and continuous non-invasive optical monitoring could have value. By providing a non-invasive

monitor sensitive to the acute cerebral physiological effects of TBI, we believe that optics can open the possibility for the development of novel treatment strategies. For example, continuous non-invasive optical monitoring could be used as a tool for earlier detection of neurological adverse conditions, or to assess treatment efficacy. The portability of the optical methods also makes them potentially useful for out-of-hospital scenarios. Importantly, diffuse optics can potentially help to improve patient outcomes even beyond severe TBI cases, where most of the neuromonitoring techniques are currently focused.

4.2. Cerebral pathophysiology at 24 hours and 14 days post-injury

After TBI, patients may develop cerebral edema and undergo a phase of cerebral hypoperfusion (reduced CBF and elevated OEF) in the first 24 hours post-injury, followed by a hyperemia phase at 1-3 days after the injury [51]. Here, we observed an increase in ipsilateral and contralateral f_{H_2O} from 30 minutes to 24 hours post-injury, which may suggest brain swelling. For the 24-hours post-injury time point, water in the contralateral hemisphere, but not the ipsilateral hemisphere, significantly exceeded the pre-injury values for the contralateral hemisphere. This ipsilateral-contralateral discrepancy is surprising. It might be a consequence of the open dura at the ipsilateral site or due to errors of the homogeneous approach.

Accompanying the tissue water content changes, we also observed changes in tissue scattering, which suggests tissue structural changes at 24 hours post-injury, potentially caused by brain swelling. In homogeneous media, the scattering power (b) is inversely proportional to the size of the scatterers [52,53]. Thus, one might hypothesize that intracellular edema would lead to a smaller b, as has been seen in previous studies of closed-head injury in mice [54,55]. Herein, however, we observed an increase in b. This increase may be explained by a potential intracranial hypertension caused by brain swelling that may have resulted in an increased density of scatterers in the optically measured tissue volume due to a compression of the cells/organelles (and thus a reduction in the scatterer size). Future work is needed to confirm and understand the structural causes of the observed scattering changes.

At 24 hours post-injury, OEF remained unaltered compared to pre-injury levels and we found no clear evidence of ischemia (reduced CBF and elevated OEF) or hyperemia (decreased OEF and elevated CBF) [56]. There is evidence, however, that oxygen metabolism started to recover, as CBF and $CMRO_2$ were no longer significantly reduced at 24 hours. However, from 30 minutes to 24 hours post injury HbT remained elevated. Coupled with the relative CBF increase over the same time period, these results may reflect a compounded effect of cerebral hemorrhage/hematoma and an inflammatory response to the injury [4,45]. Future studies with more longitudinal and continuous measurements are needed to better understand the timing of the metabolic and inflammatory responses.

Finally, at 14 days post-injury, none of the cohort-averaged cerebral metrics were different from their pre-injury levels, suggesting recovery. It's important to note, however, that our discussion has focused on comparing median pre-injury to post-injury levels. The physiology of some individual subjects substantially deviated from the median changes (ipsilateral f_{H_2O}, for example, remained elevated at 14 days post-injury in some subjects). Neuromonitoring allows for individual patient care and precision care at the right time. Future work is needed to compare individually measured physiology for individuals to brain outcomes. Indeed, to properly translate FD-DOS/DCS/bDOS for individualized TBI care, the predictive value of optics for individual patients needs to be demonstrated.

4.3. Limitations and future work

The focal impact injury model used in this study is recognized as a standard TBI model by the Federal Interagency Traumatic Brain Injury Research (FITBIR) organization, and has been extensively studied (e.g., see [32–35]). The results observed herein, however, will not be

generalizable for all human TBIs, where the pathophysiology across subjects is known to be heterogeneous [4–6]. We think our results are most applicable for penetrating or impact injuries where rupture of the dura-matter may occur. Future studies examining the cerebral physiological effects with other TBI models (e.g., rotational injury models) are important for elucidation of the complex pathophysiology of TBI across different injury types. Further, we unfortunately were unable to directly measure intracranial pressure (ICP) in this study, and there is limited information in the literature about ICP in this injury model (e.g., see [33]). To better understand the pathophysiology of this injury model, future studies should directly measure ICP and correlate it to the optical estimates of cerebral physiology.

Here we assumed that the venous/arterial ratio of blood monitored by bDOS (i.e., the γ constant from Section 2.3) is constant. However, this approximation may not be valid after TBI. This assumption is a long-standing confounder in the use of optical methods to estimate oxygen metabolism that has not yet been resolved. For example, a prior study found that this assumption could lead to errors of 9 to 21% in the calculation of relative $CMRO_2$ changes for plausible compartment blood volume fraction changes that occur during cerebral ischemia [39]. Importantly, a possible breakdown of the assumption of constant γ could explain the large variance and absence of significant changes in OEF/StO_2. In the future, studies aiming to develop methodologies that directly estimate the venous/arterial ratio are needed to improve accuracy of the optical estimates.

Furthermore, in our animal model it was necessary to use relatively high doses of isoflurane (2%) to maintain adequate sedation. Isoflurane is expected to reduce absolute cerebral metabolism [57,58] and is a potential confounder of our study. To minimize confounding, subjects were anesthetized with similar amounts of isoflurane during all optical measurements. Thus, our analysis assumes that changes in $CMRO_2$ due to injury are significantly greater than changes attributed to variability in anesthesia and anesthetic response. However, future studies should aim to investigate the effects of anesthesia on the optical estimates of cerebral physiology after TBI.

This study's proof-of-concept data suggests that FD-DOS/DCS/bDOS signals are sensitive to the cerebral physiologic effects of TBI. The inter-subject variance, however, is too large for individual diagnosis (e.g., of hematoma, edema, ischemia). The use of a semi-infinite homogeneous tissue model to recover the cerebral properties from a highly heterogeneous pig head is expected to provide the correct trends in the cerebral physiology [10,11], but this approximation can lead to misinterpretation due to assignment of changes in the scalp/skull to cerebral changes. For example, the relatively small HbT estimates reported here could be explained by an influence from the extracerebral tissues, which are expected to have smaller concentrations of hemoglobin [40,59]. This error is likely worse for tissue scattering, as the sensitivity of the optical signals to scattering in deep tissues is lower than that of absorption [60]. Importantly the scalp-to-brain distances in the subjects measured in this study was very similar to the expected values for human adults (i.e., between 1.4 and 1.7 cm) [61], where the use of the homogeneous approximation is commonly used. Important future work is needed to develop and demonstrate improved analysis algorithms that use multi-layer or realistic head models, potentially leveraging the information from MRI/CT scans, to provide a better estimate of the cerebral physiological parameters [59,62–67]. Boosting measurement signal-to-noise to reduce noise-induced crosstalk between the fitting parameters is another area of future work.

One minor limitation of the present study is that the maximum source-detector separations for DCS compared to FD-DOS/bDOS were different; the DCS separation was 0.5 cm shorter. Note, however, that the depth sensitivity of DCS is greater than DOS (for the same separation) [40], which mitigates a potential confound due to different depth sensitivities. Regardless, future work should be expected to take advantage of new strategies that boost DCS SNR [68–81] to increase DCS separations. Furthermore, in this study we opted to use modest data quality criteria for extracting the optical properties from FD-DOS (i.e., $R^2 > 0.9$). Although a case can be made to

use stricter criteria (e.g., $R^2 \geq 0.95$), this would only lead to the exclusion of a single animal at the ipsilateral 14-days post-injury timepoint and does not impact our conclusions.

Another limitation of this study is related to the hand-held spot measurements, which may have increased variability. Although we attempted to standardize the measurement location using anatomical features of the pig skull, there can still be small deviations in measurement location across the different timepoints that may have contributed to the observed variability. Further, the assumption that tissue absorbers are only hemoglobin, water, and fat is also a limitation. For example, pig scalp and skull are expected to have a significant concentration of collagen, which has a significant absorption in the near-infrared range [82]. In addition, cytochrome-c oxidase is also expected to contribute, although to a lesser extent, to tissue absorption in the near-infrared range [83]. Future studies are needed to verify the presence of additional relevant absorbers in the pig head. Finally, although encouraging, the results reported here are based on a relatively small number of animals, and further studies with larger sample sizes are warranted.

5. Conclusion

We integrated frequency-domain diffuse optical spectroscopy, diffuse correlation spectroscopy, and broadband diffuse optical spectroscopy to characterize cerebral pathophysiology in a high-fidelity adult swine model of mild-to-moderate impact TBI. Ipsilateral cerebral oxygen metabolism and blood flow acutely decreased in response to the injury, but subsequently recovered to pre-injury levels at 14 days post-injury. Tissue water volume fraction measurements revealed that edema (brain swelling) developed between 30 minutes and 24 hours post-injury. Additionally, elevated total hemoglobin concentration at 30 minutes may be indicative of cerebral hemorrhage/hematoma. At 24-hours post-injury, the associated increase in total hemoglobin and the return of cerebral blood flow to pre-injury levels may represent a compounded effect of cerebral hemorrhage/hematoma and an inflammatory response. All cerebral metrics recovered to their pre-injury levels at 14 days post-injury in this moderate injury subtype. Future work is needed to relate cerebral metrics to brain outcomes across severities of disease and differing mechanisms, such as rotational non-impact injury.

Disclosures. The authors disclose partial ownership of the following patents. Pending: WO2021/091961 [TSK, DJL, WBB, AGY, TJK], 63/257685 [WBB, DJL, TSK, TJK, RMF], WO2013/090658Al [AGY], PCT/US2012/069626 [AGY], PCT/US2015/017286 [AGY], PCT/US2015/017277 [AGY]. US8082015 [AGY], US10064554 [AGY], US10342488 [WBB and AGY], US10827976 [WBB, DJL, AGY]. No author currently receives royalties or payments from these patents.

Data availability. Data underlying the results presented in this paper are not publicly available at this time but may be obtained from the authors upon reasonable request.

References

1. J. Daugherty, "Differences in State Traumatic Brain Injury–Related Deaths, by Principal Mechanism of Injury, Intent, and Percentage of Population Living in Rural Areas: United States, 2016–2018," MMWR Morb. Mortal. Wkly. Rep. **70**(41), 1447–1452 (2021).
2. J. Daugherty, "Traumatic Brain Injury–Related Deaths by Race/Ethnicity, Sex, Intent, and Mechanism of Injury — United States, 2000–2017," MMWR Morb. Mortal. Wkly. Rep. **68**(46), 1050–1056 (2019).
3. B. E. Masel and D. S. DeWitt, "Traumatic brain injury: a disease process, not an event," Journal of Neurotrauma **27**(8), 1529–1540 (2010).
4. C. Werner and K. Engelhard, "Pathophysiology of traumatic brain injury," Br. J. Anaesth. **99**(1), 4–9 (2007).
5. N. Carney, A. M. Totten, C. O'Reilly, J. S. Ullman, G. W. J. Hawryluk, M. J. Bell, S. L. Bratton, R. Chesnut, O. A. Harris, N. Kissoon, A. M. Rubiano, L. Shutter, R. C. Tasker, M. S. Vavilala, J. Wilberger, D. W. Wright, and J. Ghajar, "Guidelines for the Management of Severe Traumatic Brain Injury, Fourth Edition," Neurosurgery **80**(1), 6–15 (2017).
6. P. M. Kochanek, R. C. Tasker, N. Carney, A. M. Totten, P. D. Adelson, N. R. Selden, C. Davis-O'Reilly, E. L. Hart, M. J. Bell, S. L. Bratton, G. A. Grant, N. Kissoon, K. E. Reuter-Rice, M. S. Vavilala, and M. S. Wainwright, "Guidelines

for the Management of Pediatric Severe Traumatic Brain Injury, Third Edition," Pediatric Critical Care Medicine **20**(3), S1–S82 (2019).

7. O. L. Cremer, G. W. van Dijk, E. van Wensen, G. J. F. Brekelmans, K. G. M. Moons, L. P. H. Leenen, and C. J. Kalkman, "Effect of intracranial pressure monitoring and targeted intensive care on functional outcome after severe head injury," Crit. Care Med. **33**(10), 2207–2213 (2005).

8. S.-S. Lang, N. K. Kumar, C. Zhao, D. Y. Zhang, A. M. Tucker, P. B. Storm, G. G. Heuer, A. A. Gajjar, C. T. Kim, I. Yuan, S. Sotardi, T. J. Kilbaugh, and J. W. Huh, "Invasive brain tissue oxygen and intracranial pressure (ICP) monitoring versus ICP-only monitoring in pediatric severe traumatic brain injury," Journal of Neurosurgery: Pediatrics **30**(2), 239–249 (2022).

9. D. O. Okonkwo, L. A. Shutter, C. Moore, N. R. Temkin, A. M. Puccio, C. J. Madden, N. Andaluz, R. M. Chesnut, M. R. Bullock, G. A. Grant, J. McGregor, M. Weaver, J. Jallo, P. D. LeRoux, D. Moberg, J. Barber, C. Lazaridis, and R. R. Diaz-Arrastia, "Brain Oxygen Optimization in Severe Traumatic Brain Injury Phase-II: A Phase II Randomized Trial*," Crit. Care Med. **45**(11), 1907–1914 (2017).

10. H. Ayaz, W. B. Baker, and G. Blaney, *et al.*, "Optical imaging and spectroscopy for the study of the human brain: status report," Neurophoton. 9(S2), (2022).

11. T. Durduran, R. Choe, W. B. Baker, and A. G. Yodh, "Diffuse optics for tissue monitoring and tomography," Rep. Prog. Phys. **73**(7), 076701 (2010).

12. T. Durduran and A. G. Yodh, "Diffuse correlation spectroscopy for non-invasive, micro-vascular cerebral blood flow measurement," NeuroImage **85**, 51–63 (2014).

13. W. Weigl, D. Milej, D. Janusek, S. Wojtkiewicz, P. Sawosz, M. Kacprzak, A. Gerega, R. Maniewski, and A. Liebert, "Application of optical methods in the monitoring of traumatic brain injury: A review," J. Cereb. Blood Flow Metab. **36**(11), 1825–1843 (2016).

14. D. J. Davies, Z. Su, M. T. Clancy, S. J. E. Lucas, H. Dehghani, A. Logan, and A. Belli, "Near-Infrared Spectroscopy in the Monitoring of Adult Traumatic Brain Injury: A Review," Journal of Neurotrauma **32**(13), 933–941 (2015).

15. S. Fantini and A. Sassaroli, "Frequency-Domain Techniques for Tissue Spectroscopy and Imaging," in *Handbook of Optical Biomedical Diagnostics, Second Edition, Volume 1: Light-Tissue Interaction* (SPIE PRESS, 2016).

16. D. Milej, A. Rajaram, M. Suwalski, L. B. Morrison, L. N. Shoemaker, and K. St. Lawrence, "Assessing the relationship between the cerebral metabolic rate of oxygen and the oxidation state of cytochrome-c-oxidase," Neurophoton. 9(03), (2022).

17. A. Rajaram, D. Milej, M. Suwalski, L. Kebaya, M. Kewin, L. Yip, S. de Ribaupierre, V. Han, M. Diop, S. Bhattacharya, and K. St. Lawrence, "Assessing cerebral blood flow, oxygenation and cytochrome c oxidase stability in preterm infants during the first 3 days after birth," Sci. Rep. **12**(1), 181 (2022).

18. A. Rajaram, G. Bale, M. Kewin, L. B. Morrison, I. Tachtsidis, K. St. Lawrence, and M. Diop, "Simultaneous monitoring of cerebral perfusion and cytochrome c oxidase by combining broadband near-infrared spectroscopy and diffuse correlation spectroscopy," Biomed. Opt. Express **9**(6), 2588 (2018).

19. A. Rajaram, D. Milej, M. Suwalski, L. C. M. Yip, L. R. Guo, M. W. A. Chu, J. Chui, M. Diop, J. M. Murkin, and K. St. Lawrence, "Optical monitoring of cerebral perfusion and metabolism in adults during cardiac surgery with cardiopulmonary bypass," Biomed. Opt. Express **11**(10), 5967 (2020).

20. T. S. Ko, C. D. Mavroudis, and W. B. Baker, *et al.*, "Non-invasive optical neuromonitoring of the temperature-dependence of cerebral oxygen metabolism during deep hypothermic cardiopulmonary bypass in neonatal swine," J. Cereb. Blood Flow Metab. **40**(1), 187–203 (2020).

21. R. M. Forti, M. Katsurayama, J. Menko, L. Valler, A. Quiroga, A. L. E. Falcão, L. M. Li, and R. C. Mesquita, "Real-time non-invasive assessment of cerebral hemodynamics with diffuse optical spectroscopies in a neuro intensive care unit: an observational case study," Front. Med. **7**, 147 (2020).

22. V. Jain, E. M. Buckley, D. J. Licht, J. M. Lynch, P. J. Schwab, M. Y. Naim, N. A. Lavin, S. C. Nicolson, L. M. Montenegro, A. G. Yodh, and F. W. Wehrli, "Cerebral oxygen metabolism in neonates with congenital heart disease quantified by MRI and optics," J. Cereb. Blood Flow Metab. **34**(3), 380–388 (2014).

23. J. M. Lynch, C. D. Mavroudis, T. S. Ko, M. Jacobwitz, D. R. Busch, R. Xiao, S. C. Nicolson, L. M. Montenegro, J. W. Gaynor, A. G. Yodh, and D. J. Licht, "Association of Ongoing Cerebral Oxygen Extraction During Deep Hypothermic Circulatory Arrest With Postoperative Brain Injury," Semin. Thorac. Cardiovasc. Surg. **34**(4), 1275–1284 (2022).

24. J. M. Lynch, T. Ko, D. R. Busch, J. J. Newland, M. E. Winters, K. Mensah-Brown, T. W. Boorady, R. Xiao, S. C. Nicolson, L. M. Montenegro, J. W. Gaynor, T. L. Spray, A. G. Yodh, M. Y. Naim, and D. J. Licht, "Preoperative cerebral hemodynamics from birth to surgery in neonates with critical congenital heart disease," J. Thorac. Cardiovasc. Surg. **156**(4), 1657–1664 (2018).

25. H. H. Cheng, S. L. Ferradal, R. Vyas, D. Wigmore, E. McDavitt, J. S. Soul, M. A. Franceschini, J. W. Newburger, and P. E. Grant, "Abnormalities in cerebral hemodynamics and changes with surgical intervention in neonates with congenital heart disease," J. Thorac. Cardiovasc. Surg. **159**(5), 2012–2021 (2020).

26. N. Roche-Labarbe, A. Fenoglio, A. Aggarwal, M. Dehaes, S. A. Carp, M. A. Franceschini, and P. E. Grant, "Near-infrared spectroscopy assessment of cerebral oxygen metabolism in the developing premature brain," J. Cereb. Blood Flow Metab. **32**(3), 481–488 (2012).

27. A. I. Zavriyev, K. Kaya, P. Farzam, P. Y. Farzam, J. Sunwoo, A. S. Jassar, T. M. Sundt, S. A. Carp, M. A. Franceschini, and J. Z. Qu, "The role of diffuse correlation spectroscopy and frequency-domain near-infrared spectroscopy in monitoring cerebral hemodynamics during hypothermic circulatory arrests," JTCVS Tech. **7**, 161–177 (2021).

28. J. M. Cochran, S. H. Chung, A. Leproux, W. B. Baker, D. R. Busch, A. M. DeMichele, J. Tchou, B. J. Tromberg, and A. G. Yodh, "Longitudinal optical monitoring of blood flow in breast tumors during neoadjuvant chemotherapy," Phys. Med. Biol. **62**(12), 4637–4653 (2017).

29. N. A. Martin, R. V. Patwardhan, M. J. Alexander, C. Z. Africk, J. H. Lee, E. Shalmon, D. A. Hovda, and D. P. Becker, "Characterization of cerebral hemodynamic phases following severe head trauma: hypoperfusion, hyperemia, and vasospasm," J. Neurosurg. **87**(1), 9–19 (1997).

30. C. Zhou, S. A. Eucker, T. Durduran, G. Yu, J. Ralston, S. H. Friess, R. N. Ichord, S. S. Margulies, and A. G. Yodh, "Diffuse optical monitoring of hemodynamic changes in piglet brain with closed head injury," J. Biomed. Opt. **14**(3), 034015 (2009).

31. S. H. Friess, J. Ralston, S. A. Eucker, M. A. Helfaer, C. Smith, and S. S. Margulies, "Neurocritical care monitoring correlates with neuropathology in a swine model of pediatric traumatic brain injury," Neurosurgery **69**(5), 1139–1147 (2011).

32. A.-C. Duhaime, S. S. Margulies, S. R. Durham, M. M. O'Rourke, J. A. Golden, S. Marwaha, and R. Raghupathi, "Maturation-dependent response of the piglet brain to scaled cortical impact," J. Neurosurg. **93**(3), 455–462 (2000).

33. G. T. Manley, G. Rosenthal, M. Lam, D. Morabito, D. Yan, N. Derugin, A. Bollen, M. M. Knudson, and S. S. Panter, "Controlled cortical impact in swine: pathophysiology and biomechanics," Journal of Neurotrauma **23**(2), 128–139 (2006).

34. T. J. Kilbaugh, M. Karlsson, M. Byro, A. Bebee, J. Ralston, S. Sullivan, A.-C. Duhaime, M. J. Hansson, E. Elmér, and S. S. Margulies, "Mitochondrial bioenergetic alterations after focal traumatic brain injury in the immature brain," Exp. Neurol. **271**, 136–144 (2015).

35. M. Karlsson, B. Pukenas, S. Chawla, J. K. Ehinger, R. Plyler, M. Stolow, M. Gabello, M. Hugerth, E. Elmér, M. J. Hansson, S. Margulies, and T. Kilbaugh, "Neuroprotective effects of cyclosporine in a porcine pre-clinical trial of focal traumatic brain injury," Journal of Neurotrauma **36**(1), 14–24 (2019).

36. S. A. Carp, P. Farzam, N. Redes, D. M. Hueber, and M. A. Franceschini, "Combined multi-distance frequency domain and diffuse correlation spectroscopy system with simultaneous data acquisition and real-time analysis," Biomed. Opt. Express **8**(9), 3993 (2017).

37. D. M. Hueber, M. A. Franceschini, H. Y. Ma, Q. Zhang, J. R. Ballesteros, S. Fantini, D. Wallace, V. Ntziachristos, and B. Chance, "Non-invasive and quantitative near-infrared haemoglobin spectrometry in the piglet brain during hypoxic stress, using a frequency-domain multidistance instrument†," Phys. Med. Biol. **46**(1), 41–62 (2001).

38. F. Bevilacqua, A. J. Berger, A. E. Cerussi, D. Jakubowski, and B. J. Tromberg, "Broadband absorption spectroscopy in turbid media by combined frequency-domain and steady-state methods," Appl. Opt. **39**(34), 6498 (2000).

39. J. P. Culver, T. Durduran, D. Furuya, C. Cheung, J. H. Greenberg, and A. G. Yodh, "Diffuse Optical Tomography of Cerebral Blood Flow, Oxygenation, and Metabolism in Rat during Focal Ischemia," J. Cereb. Blood Flow Metab. **23**(8), 911–924 (2003).

40. J. Selb, D. A. Boas, S.-T. Chan, K. C. Evans, E. M. Buckley, and S. A. Carp, "Sensitivity of near-infrared spectroscopy and diffuse correlation spectroscopy to brain hemodynamics: simulations and experimental findings during hypercapnia," Neurophotonics **1**(1), 015005 (2014).

41. A. A. Middleton and D. S. Fisher, "Discrete scatterers and autocorrelations of multiply scattered light," Phys. Rev. B **43**(7), 5934–5938 (1991).

42. H.-M. Wu, S.-C. Huang, N. Hattori, T. C. Glenn, P. M. Vespa, C.-L. Yu, D. A. Hovda, M. E. Phelps, and M. Bergsneider, "Selective Metabolic Reduction in Gray Matter Acutely following Human Traumatic Brain Injury," Journal of Neurotrauma **21**(2), 149–161 (2004).

43. R. M. Jha, P. M. Kochanek, and J. M. Simard, "Pathophysiology and treatment of cerebral edema in traumatic brain injury," Neuropharmacology **145**, 230–246 (2019).

44. J. A. Stokum, V. Gerzanich, and J. M. Simard, "Molecular pathophysiology of cerebral edema," J. Cereb. Blood Flow Metab. **36**(3), 513–538 (2016).

45. Y. Onetti, A. P. Dantas, B. Pérez, R. Cugota, A. Chamorro, A. M. Planas, E. Vila, and F. Jiménez-Altayó, "Middle cerebral artery remodeling following transient brain ischemia is linked to early postischemic hyperemia: A target of uric acid treatment," Am. J. Physiol. Heart Circ. Physiol. **308**(8), H862–H874 (2015).

46. C. S. Kidwell and M. Wintermark, "Imaging of intracranial haemorrhage," Lancet Neurol. **7**(3), 256–267 (2008).

47. J. Peters, B. Van Wageningen, N. Hoogerwerf, and E. Tan, "Near-infrared spectroscopy: a promising prehospital tool for management of traumatic brain injury," Prehosp. Disaster med. **32**(4), 414–418 (2017).

48. H. Ayaz, M. Izzetoglu, K. Izzetoglu, B. Onaral, and B. Ben Dor, "Early diagnosis of traumatic intracranial hematomas," J. Biomed. Opt. **24**(05), 1 (2019).

49. M. E. Ryan, S. Pruthi, and N. K. Desai, *et al.*, "ACR Appropriateness Criteria® Head Trauma-Child," J. Am. Coll. Radiol. **17**(5), S125–S137 (2020).

50. R. Y. Shih, J. Burns, A. A. Ajam, J. S. Broder, S. Chakraborty, A. T. Kendi, M. E. Lacy, L. N. Ledbetter, R. K. Lee, D. S. Liebeskind, J. M. Pollock, J. A. Prall, T. Ptak, P. B. Raksin, M. D. Shaines, A. J. Tsiouris, P. S. Utukuri, L. L. Wang, and A. S. Corey, "ACR Appropriateness Criteria® Head Trauma: 2021 Update," J. Am. Coll. Radiol. **18**(5), S13–S36 (2021).

51. C. Sokoloff, D. Williamson, K. Serri, M. Albert, C. Odier, E. Charbonney, and F. Bernard, and for the ÉRESI Reseach Group (Équipe de Recherche En Soins Intensifs), "Clinical Usefulness of Transcranial Doppler as a Screening Tool

for Early Cerebral Hypoxic Episodes in Patients with Moderate and Severe Traumatic Brain Injury," Neurocrit Care **32**(2), 486–491 (2020).

52. J. R. Mourant, T. Fuselier, J. Boyer, T. M. Johnson, and I. J. Bigio, "Predictions and measurements of scattering and absorption over broad wavelength ranges in tissue phantoms," Appl. Opt. **36**(4), 949 (1997).

53. J. R. Mourant, J. P. Freyer, A. H. Hielscher, A. A. Eick, D. Shen, and T. M. Johnson, "Mechanisms of light scattering from biological cells relevant to noninvasive optical-tissue diagnostics," Appl. Opt. **37**(16), 3586 (1998).

54. D. Abookasis, B. Volkov, and M. S. Mathews, "Closed head injury-induced changes in brain pathophysiology assessed with near-infrared structured illumination in a mouse model," J. Biomed. Opt **18**(11), 116007 (2013).

55. D. Abookasis, A. Sochat, and M. S. Mathews M.D, "Monitoring hemodynamic and morphologic responses to closed head injury in a mouse model using orthogonal diffuse near-infrared light reflectance spectroscopy," J. Biomed. Opt **18**(4), 045003 (2013).

56. W. B. Baker, R. Balu, L. He, V. C. Kavuri, D. R. Busch, O. Amendolia, F. Quattrone, S. Frangos, E. Maloney-Wilensky, K. Abramson, E. Mahanna Gabrielli, A. G. Yodh, and W. Andrew Kofke, "Continuous non-invasive optical monitoring of cerebral blood flow and oxidative metabolism after acute brain injury," J. Cereb. Blood Flow Metab. **39**(8), 1469–1485 (2019).

57. T. Oshima, F. Karasawa, Y. Okazaki, H. Wada, and T. Satoh, "Effects of sevoflurane on cerebral blood flow and cerebral metabolic rate of oxygen in human beings: a comparison with isoflurane," Eur. J. Anaesthesiol. **20**(7), 543–547 (2003).

58. A. M. Slupe and J. R. Kirsch, "Effects of anesthesia on cerebral blood flow, metabolism, and neuroprotection," J. Cereb. Blood Flow Metab. **38**(12), 2192–2208 (2018).

59. B. Hallacoglu, A. Sassaroli, and S. Fantini, "Optical characterization of two-layered turbid media for non-invasive, absolute oximetry in cerebral and extracerebral tissue," PLoS One **8**(5), e64095 (2013).

60. J. Selb, T. M. Ogden, J. Dubb, Q. Fang, and D. A. Boas, "Comparison of a layered slab and an atlas head model for Monte Carlo fitting of time-domain near-infrared spectroscopy data of the adult head," J. Biomed. Opt **19**(1), 016010 (2014).

61. M. M. Wu, K. Perdue, S.-T. Chan, K. A. Stephens, B. Deng, M. A. Franceschini, and S. A. Carp, "Complete head cerebral sensitivity mapping for diffuse correlation spectroscopy using subject-specific magnetic resonance imaging models," Biomed. Opt. Express **13**(3), 1131 (2022).

62. M. M. Wu, S.-T. Chan, D. Mazumder, D. Tamborini, K. A. Stephens, B. Deng, P. Farzam, J. Y. Chu, M. A. Franceschini, J. Z. Qu, and S. A. Carp, "Improved accuracy of cerebral blood flow quantification in the presence of systemic physiology cross-talk using multi-layer Monte Carlo modeling," Neurophoton. **8**(1), 015001 (2021).

63. H. Zhao, E. Sathialingam, and E. M. Buckley, "Accuracy of diffuse correlation spectroscopy measurements of cerebral blood flow when using a three-layer analytical model," Biomed. Opt. Express **12**(11), 7149 (2021).

64. H. Dehghani, M. E. Eames, P. K. Yalavarthy, S. C. Davis, S. Srinivasan, C. M. Carpenter, B. W. Pogue, and K. D. Paulsen, "Near infrared optical tomography using NIRFAST: Algorithm for numerical model and image reconstruction," Commun. Numer. Meth. Engng. **25**(6), 711–732 (2009).

65. J. Wu, S. Tabassum, W. L. Brown, S. Wood, J. Yang, and J. M. Kainerstorfer, "Two-layer analytical model for estimation of layer thickness and flow using Diffuse Correlation Spectroscopy," PLoS One **17**(9), e0274258 (2022).

66. D. Milej, A. Abdalmalak, A. Rajaram, and K. St. Lawrence, "Direct assessment of extracerebral signal contamination on optical measurements of cerebral blood flow, oxygenation, and metabolism," Neurophoton. **7**(1), 045002 (2020).

67. Q. Fang, "Mesh-based Monte Carlo method using fast ray-tracing in Plücker coordinates," Biomed. Opt. Express **1**(1), 165 (2010).

68. W. Liu, R. Qian, S. Xu, P. Chandra Konda, J. Jönsson, M. Harfouche, D. Borycki, C. Cooke, E. Berrocal, Q. Dai, H. Wang, and R. Horstmeyer, "Fast and sensitive diffuse correlation spectroscopy with highly parallelized single photon detection," APL Photonics **6**(2), 026106 (2021).

69. R. Bi, Y. Du, G. Singh, J.-H. Ho, S. Zhang, A. B. Ebrahim Attia, X. Li, and M. C. Olivo, "Fast pulsatile blood flow measurement in deep tissue through a multimode detection fiber," J. Biomed. Opt. **25**(05), 1 (2020).

70. W. Zhou, O. Kholiqov, S. P. Chong, and V. J. Srinivasan, "Highly parallel, interferometric diffusing wave spectroscopy for monitoring cerebral blood flow dynamics," Optica **5**(5), 518 (2018).

71. E. James and S. Powell, "Fourier domain diffuse correlation spectroscopy with heterodyne holographic detection," Biomed. Opt. Express **11**(11), 6755 (2020).

72. M. B. Robinson, D. A. Boas, S. Sakadzic, M. A. Franceschini, and S. A. Carp, "Interferometric diffuse correlation spectroscopy improves measurements at long source–detector separation and low photon count rate," J. Biomed. Opt. **25**(9), 097004 (2020).

73. J. Xu, A. K. Jahromi, J. Brake, J. E. Robinson, and C. Yang, "Interferometric speckle visibility spectroscopy (ISVS) for human cerebral blood flow monitoring," APL Photonics **5**(12), 126102 (2020).

74. J. Xu, A. K. Jahromi, and C. Yang, "Diffusing wave spectroscopy: A unified treatment on temporal sampling and speckle ensemble methods," APL Photonics **6**(1), 016105 (2021).

75. O. Kholiqov, W. Zhou, T. Zhang, V. N. Du Le, and V. J. Srinivasan, "Time-of-flight resolved light field fluctuations reveal deep human tissue physiology," Nat. Commun. **11**(1), 391 (2020).

76. M. B. Robinson, S. A. Carp, A. Peruch, D. A. Boas, M. A. Franceschini, and S. Sakadžić, "Characterization of continuous wave ultrasound for acousto-optic modulated diffuse correlation spectroscopy (AOM-DCS)," Biomed. Opt. Express **11**(6), 3071 (2020).

77. S. A. Carp, D. Tamborini, D. Mazumder, K.-C. Tony Wu, M. R. Robinson, K. A. Stephens, O. Shatrovoy, N. Lue, N. Ozana, M. H. Blackwell, and M. A. Franceschini, "Diffuse correlation spectroscopy measurements of blood flow using 1064 nm light," J. Biomed. Opt. **25**(9), 097003 (2020)..

78. L. Colombo, M. Pagliazzi, S. K. Venkata Sekar, D. Contini, T. Durduran, and A. Pifferi, "In vivo time-domain diffuse correlation spectroscopy above the water absorption peak," Opt. Lett. **45**(13), 3377 (2020).

79. M. Pagliazzi, S. K. V. Sekar, L. Colombo, E. Martinenghi, J. Minnema, R. Erdmann, D. Contini, A. D. Mora, A. Torricelli, A. Pifferi, and T. Durduran, "Time domain diffuse correlation spectroscopy with a high coherence pulsed source: in vivo and phantom results," Biomed. Opt. Express **8**(11), 5311 (2017).

80. S. Samaei, P. Sawosz, M. Kacprzak, Ż. Pastuszak, D. Borycki, and A. Liebert, "Time-domain diffuse correlation spectroscopy (TD-DCS) for noninvasive, depth-dependent blood flow quantification in human tissue in vivo," Sci. Rep. **11**(1), 1817 (2021).

81. J. Sutin, B. Zimmerman, D. Tyulmankov, D. Tamborini, K. C. Wu, J. Selb, A. Gulinatti, I. Rech, A. Tosi, D. A. Boas, and M. A. Franceschini, "Time-domain diffuse correlation spectroscopy," Optica **3**(9), 1006 (2016).

82. S. K. V. Sekar, I. Bargigia, A. D. Mora, P. Taroni, A. Ruggeri, A. Tosi, A. Pifferi, and A. Farina, "Diffuse optical characterization of collagen absorption from 500 to 1700nm," J. Biomed. Opt **22**(1), 015006 (2017).

83. G. Bale, C. E. Elwell, and I. Tachtsidis, "From Jöbsis to the present day: a review of clinical near-infrared spectroscopy measurements of cerebral cytochrome-c-oxidase," J. Biomed. Opt **21**(9), 091307 (2016).